# Resonant tunneling theory of planar quantum dot structures

Jian-Bai Xia and Shu-Shen Li
*Chinese Center of Advanced Science and Technology (World Laboratory), P.O. Box 8730, Beijing 100080, China*
*and Institute of Semiconductors, Chinese Academy of Sciences, P.O. Box 912, Beijing 100083, China*
(Received 25 March 2003; published 14 August 2003)

The ballistic transport in the semiconductor, planar, circular quantum dot structures is studied theoretically. The transmission probabilities show apparent resonant tunneling peaks, which correspond to energies of bound states in the dot. By use of structures with different angles between the inject and exit channels, the resonant peaks can be identified very effectively. The perpendicular magnetic field has obvious effect on the energies of bound states in the quantum dot, and thus the resonant peaks. The treatment of the boundary conditions simplifies the problem to the solution of a set of linear algebraic equations. The theoretical results in this paper can be used to design planar resonant tunneling devices, whose resonant peaks are adjustable by the angle between the inject and exit channels and the applied magnetic field. The resonant tunneling in the circular dot structures can also be used to study the bound states in the absence and presence of magnetic field.

DOI: 10.1103/PhysRevB.68.075310 PACS number(s): 73.21.La, 73.63.Kv

## I. INTRODUCTION

In the past few years, self-assembled dots have attracted considerable interest because their atomlike properties make them ideal for studying the physics of confined carriers and many-body effects. They could also lead to novel devices applications in fields such as quantum cryptography, quantum computing, optics, and optoelectronics. Altering growth condition, Garcia *et al.*[1] fabricated quantum dots with a ring shape. The decisive difference between quantum rings and quantum dots is their topology—the hole in their middle—becomes dominant when an external magnetic field is applied. The magnetic flux that penetrates the interior of the ring will then determine the nature of the electronic states. Warburton *et al.*[2] reported how the optical emission (photoluminescence) of a single ring changes abruptly whenever an electron is added to the ring, and that the sizes of the jumps reveal a shell structure. Lorke *et al.*[3] employed capacitance spectroscopy and infrared-absorption spectroscopy to investigate both the ground states and the excitations of these rings. Applying a magnetic field perpendicular to the plane of the rings, they found that, when on flux quantum threads the interior of each ring, a change in the ground state from angular momentum $m=0$ to $m=-1$ takes place. Theoretically, Llorens *et al.*[4] studied the electronic states of quantum rings under applied lateral electric field. Xia and Li[5] calculated the electronic structure and transport properties of quantum rings in a magnetic field.

In this paper, we study theoretically the electronic structure and the transport property of one kind of quantum dot structure, planar quantum dots, whose height is much smaller than their lateral size, so that we can use the adiabatic approximation where the motion along the $z$ axis is decoupled from that in the $x$-$y$ plane, and we only consider the confined states in the $x$-$y$ plane. Recent technological advances in nanometer-scale lithography and atomic-layer epitaxy which can provide semiconductor planar microstructures, whose size is smaller than the inelastic and elastic mean scattering lengths, have attracted much attention to the study of mesoscopic systems, especially after the discovery of the quantized conductance phenomenon.[6,7] Inspired by the prospect of building devices based on the quantum interference effect, many authors have proposed various structures[8] made from high mobility modulation-doped AlGaAs/GaAs heterostructures. The most prominent advantage of the quantum interference device lies in the fact that its operation is controlled by the relative phase of the electron waves and a very high switching speed can be achieved. In this paper, we study a planar circular quantum dot structure with outer potential barrier, which is schematically illustrated in Fig. 1. We first study the electronic states of an isolated planar quantum dot in the absence and presence of perpendicular magnetic field. Then we study the transport property: the electron wave is injected in the channel at the right ($\theta=0$), the wave partly exits out in the channel at the $\theta$ angle, and the rest is reflected back in the original channel. It is found that if the energy of the injected electron equals the eigenenergy of the bound state in the quantum dot, there will occur strong resonant tunneling, similar to that in usual quantum well structures with double potential barriers. The theoretical method used is the mode-matching method. By treating the boundary conditions with the method proposed by us,[9] we can transfer the problem to the solution of a set of linear algebraic equations with complex coefficients.

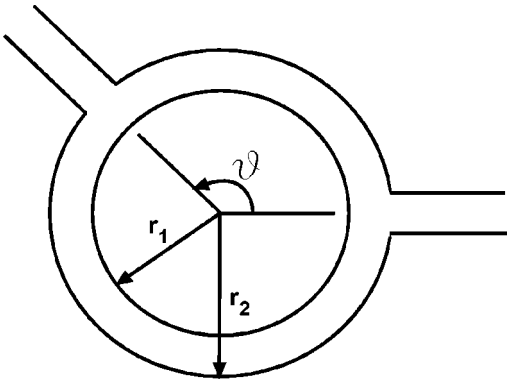


FIG. 1. Schematic illustration of the circular quantum dot and resonant tunneling structure.

 

Section II explains the theoretical model, Sec. III presents the calculated results and discussion, and Sec. IV is a summary.

## II. THEORETICAL MODEL

The equation of the radial movement of electrons in the planar quantum dot structures is given in Ref. 5. The confinement potential for the quantum dot (Fig. 1) is

$$V(r)=\begin{cases} 0, & 0\leqslant r\leqslant r_1 \\ V_0, & r_1\leqslant r\leqslant r_2 \\ \infty, & r>r_2, \end{cases} \tag{1}$$

where $V_0$ is the potential barrier height. In the absence of magnetic field, the wave function $\phi_n(r)$ can be written as

$$\phi_n(r)=J_n(kr), \quad 0<r<r_1, \tag{2}$$

$$\phi_n(r)=\alpha_n I_n(Kr)+\beta_n K_n(Kr), \quad r_1<r<r_2, \tag{3}$$

where $I_n(x)$ and $K_n(x)$ are the Bessel functions of imaginary argument,

$$k=\sqrt{\frac{2m^*E}{\hbar^2}}, \tag{4}$$

$$K=\sqrt{\frac{2m^*(V_0-E)}{\hbar^2}}. \tag{5}$$

$\alpha_n$ and $\beta_n$ are determined by the boundary conditions at the inner radius of the barrier region $r_1$. The energy of bound states is determined by

$$\alpha_m I_m(Kr_2)+\beta_m K_m(Kr_2)=0, \quad m=0,1,\ldots,M, \tag{6}$$

which demands that the wave function equals zero at the outer boundary of the potential barrier region. In the presence of perpendicular magnetic field, the wave functions in the quantum dot are given by the degenerate hypergeometric functions instead of the Bessel functions. But here we use

$$\psi_n=\frac{\sqrt{2}}{r_2 J_{m+1}(\alpha_n^m)} J_m(\alpha_n^m r/r_2) \tag{7}$$

as the basic function to expand the wave function, where $J_m(x)$ is the Bessel function of $m$th order, $\alpha_n^m$ is its $n$th zero point.

For the transport problem, the wave functions in the channel region can be written as

$$\Psi_c=\sum_{l=1}^{N} (a_l e^{ik_l x}+b_l e^{-ik_l x})\phi_l(y), \tag{8}$$

where $x$ is the coordinate along the channel outward from the central region and $y$ is the transverse coordinate. $\phi_l(y)$ is the transverse confined wave function with eigenenergy $E_l$ and $N$ is the number of transverse modes involved in the transport:

$$\phi_l(y)=\sqrt{\frac{2}{d}}\sin\frac{l\pi y}{d}, \tag{9}$$

$$E_l=\frac{\hbar^2}{2m^*}\left(\frac{l\pi}{d}\right)^2, \tag{10}$$

where $d$ is the width of channel, $k_l$ is the propagation wave vector for the $l$th transverse mode:

$$k_l=\sqrt{\frac{2m^*(E-E_l)}{\hbar^2}}, \tag{11}$$

with $E$ the electron energy, and $k_l$ can be imaginary.

The wave function for the quantum dot region (Fig. 1) can be written as

$$\Psi_a=\sum_{n=-M}^{M} c_n\phi_n(r)e^{in\theta}/\sqrt{2\pi}, \tag{12}$$

where $\phi_n(r)$ is the radial wave function (3). In real calculation, we use the numerical integration to calculate the radial functions.

At the interface between the channel and the central region, the wave functions have to satisfy the boundary conditions.

$$\sum_{l=1}^{N}(a_l+b_l)\phi_l(y)+\sum_{l=1}^{N}(a_l'+b_l')\phi_l(y') =\sum_{n=0}^{M} c_n\phi_n(r_2)e^{in\theta}/\sqrt{2\pi}, \tag{13}$$

$$\sum_{l=1}^{N} ik_l(a_l-b_l)\phi_l(y)+\sum_{l=1}^{N} ik_l(a_l'-b_l')\phi_l(y') =\sum_{n=0}^{M} c_n\phi_n'(r_2)e^{in\theta}/\sqrt{2\pi}, \tag{14}$$

where $r_2$ is the outside radius, $a_l$, $b_l$ and $a_l'$, $b_l'$ are coefficients of wave functions in the electron going in and out channels, respectively. According to the method in Ref. 9, we multiply the two sides of Eq. (13) by $e^{-im\theta}/\sqrt{2\pi}$ and integrate for $\theta$ from 0 to $2\pi$. Here we neglect the difference between the straight line of the channel and the arc line of the ring, the coordinate $y$ can be changed to $r_2\theta$, and the normalization constant of the transverse wave function (9) is changed to $\sqrt{2r_2/d}$. The two sides of the two channels correspond to angles $\theta_1$ and $\theta_2$, $\theta_3$ and $\theta_4$, respectively, then we obtain

$$\sum_{l=1}^{N}(a_l+b_l)I_{-ml}+\sum_{l=1}^{N}(a_l'+b_l')I'_{-ml}=c_m\phi_m(r_2), \quad m=0,\pm1,\pm2,\ldots,\pm M. \tag{15}$$

By multiplying the two sides of Eq. (14) by $\phi_n(y)$ and integrating for $\theta$ from $\theta_1$ to $\theta_2$, we obtain

$$ik_n(a_n-b_n)=\sum_{m=0}^{M} c_m\phi'_m(r_2)I_{mn}, \qquad n=1,2,\ldots,N. \tag{16}$$

And by multiplying the two sides of Eq. (14) by $\phi_n(y')$ and integrating for $\theta$ from $\theta_3$ to $\theta_4$, we obtain

$$ik_n(a'_n-b'_n)=\sum_{m=0}^{M} c_m\phi'_m(r_2)I'_{mn}, \qquad n=1,2,\ldots,N, \tag{17}$$

where

$$I_{mn}=\sqrt{\frac{r_2}{\pi d}}\int_{\theta_1}^{\theta_2}\sin\frac{n\pi r_2(\theta-\theta_1)}{d}e^{im\theta}d\theta, \tag{18}$$

$$I'_{mn}=\sqrt{\frac{r_2}{\pi d}}\int_{\theta_3}^{\theta_4}\sin\frac{n\pi r_2(\theta-\theta_3)}{d}e^{im\theta}d\theta. \tag{19}$$

If there are $2M+1$ Bessel functions involved in the summation of Eq. (12) and $N$ transverse states involved in the summation of Eq. (8), then we obtain $2M+2N+1$ equations. In Eqs. (15)–(17), $b_n$ and $b'_n$ are coefficients of electron waves traveling inwards or increasing exponentially with $x$ (for imaginary $k_n$), which are all set to be zero according to a physical consideration, except one coefficient $b_i=1/\sqrt{k_i}$, representing the amplitude of one injected wave. There are $2M+2N+1$ unknown coefficients in Eqs. (15)–(17): $a_n, a'_n$ $(n=1,2,\ldots,N)$ and $c_m$ $(m=0,\pm1,\ldots,\pm M)$, therefore the set of equations is complete and unique.

Solving the set of equations we obtain the coefficients $a_n, a'_n$, which are related to the transmission and reflection amplitudes,

$$a_n=\frac{r_{ni}}{k_n}, \tag{20}$$

$$a'_n=\frac{t_{ni}}{k_n}. \tag{21}$$

The total transmission and reflection probabilities are given by

$$T=\sum_{ij}|t_{ij}|^2, \tag{22}$$

$$R=\sum_{ij}|r_{ij}|^2, \tag{23}$$

and

$$T+R=N_t, \tag{24}$$

where the summation is over all the traveling states in the channel, i.e., for all states with $E_i<E$, $E_i$ is given by Eq. (10). $N_t$ is the number of traveling states. The coefficients $c_m$ are simultaneously obtained, which give the wave function in the central region for a definite energy $E$ [Eq. (12)]. In our calculation, the numbers of excited states involved in the calculation is five for the channel [Eq. (8)], and the wave function for the central region [Eq. (12)] is expanded up to twentieth order of angular momentum quantum number.

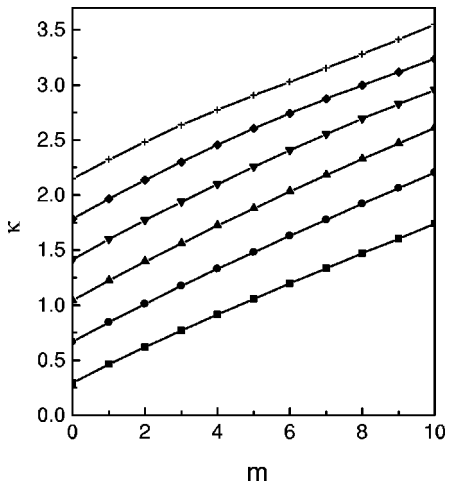


FIG. 2. Electron momentum as a function of the angular momentum $m$ in $b=0$. The curves from down to up correspond to the ground, the first excited, the second excited states, etc., respectively.

## III. RESULTS AND DISCUSSION

In the calculation, we use the width of the channel $d$ as the unit of length, the energy of the first transverse state in the channel [$n=1$ in Eq. (9)] as the unit of energy $E_0$, the electron momentum $\kappa=\sqrt{E}$ to represent the energy $E$ (in units of $E_0$), and

$$b=\frac{\hbar eB}{m^*c}/E_0 \tag{25}$$

as the unit of magnetic-field strength. For definition, we calculated the planar quantum dot with the inner and outside radii $r_1=2.5$, $r_2=3$, and $V_0=5$.

### A. Electronic states

Figure 2 shows the electron momentum $\kappa$ as functions of the angular momentum $m$ in the absence of magnetic field. From Fig. 2, we see that $\kappa$ vary basically linearly with $m$. Figure 3 shows $\kappa$ as functions of the magnetic field $b$ for $m=0$ and $\pm7$ states. From Fig. 3, we see that at $b=0$, $\kappa$ of $m=\pm7$ states are degenerate, and larger than those of $m=0$ state, as shown in Fig. 2. As $b$ increases, the degeneracy of $\pm m$ states is lifted, and all $-m$ states (including $m=0$ state) approach to a common limit. It occurs at about $b=2$. Figure 4 shows $\kappa$ as functions of the angular momentum $m$ in the magnetic field of $b=1$ and $b=4$, respectively. From Fig. 4, we see that for $b=4$, $\kappa$ of $-m$ states are basically constant, independent of $-m$ value, while for $b=1$ $\kappa$ of $-m$ states are different, dependent on the $-m$ value. This result was found early by Sikorski and Merkt,[10] who studied variation of the energy levels of InSb quantum dot with magnetic field, using parabolic potential as the confinement potential. They obtained the eigenenergy

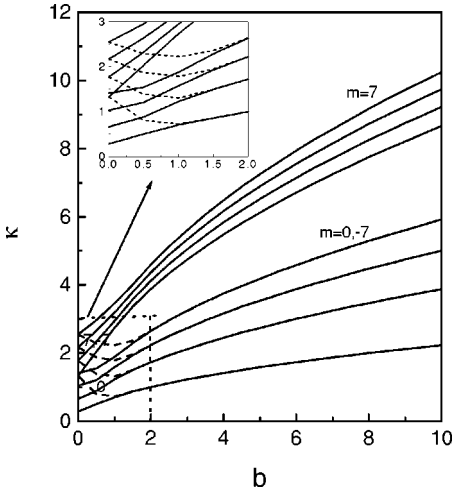


FIG. 3. Electron momentum as a function of the magnetic field $b$ for $m=0$ and $\pm 7$ states.

$$E_{nm}=\left(n+\frac{|m|}{2}+\frac{1}{2}\right)\omega+\frac{m}{2}\omega_c, \tag{26}$$

where $\omega^2=\omega_c^2+4\omega_0^2$, $\omega_c$ and $\omega_0$ are circular frequencies of the magnetic field and the confinement potential, respectively. From Eq. (26), we see that when $\omega_c \gg \omega_0$, $E_{nm}\rightarrow(n+\frac{1}{2})\omega_c$ for $m\leqslant 0$ states. This result is also valid for other circular quantum dots with arbitrary confinement potential.

### B. Coulomb energy of two electrons

Figure 5 shows the Coulomb energies of two electrons $E_c$ as functions of the magnetic field $b$ for $m=0$ and $m=4$ states, respectively. The unit of the Coulomb energy is $e^2/\varepsilon_0 d$. From Fig. 5, we see that the Coulomb energies $E_c$ increase with the magnetic field $b$ increasing. Because the magnetic field produces a parabolic potential, the larger is the magnetic field, the closer is the electron wave function located in the center region, resulting in increase of the Coulomb energy. The increase of $E_c$ of the $m=0$ state is larger than that of the $m=4$ state. It is noticed that in the presence of magnetic field, though the eigenenergy ($\kappa$) is different for $\pm m$ states, the wave functions are the same, therefore the Coulomb energies are also the same for $\pm m$ states. Figure 6 shows $E_c$ as functions of $m$ for $b=0$ and $b=4$, respectively. From Fig. 6, we see that the Coulomb energies $E_c$ decrease with $m$ increasing, and the ones in the presence of magnetic field ($b=4$) are much larger than those at $b=0$. The wave function of a larger $m$ state is distributed in the outer region, while the wave function of a smaller $m$ state is distributed in the center region, therefore the Coulomb energy of the smaller $m$ state is larger than that of the larger $m$ state.

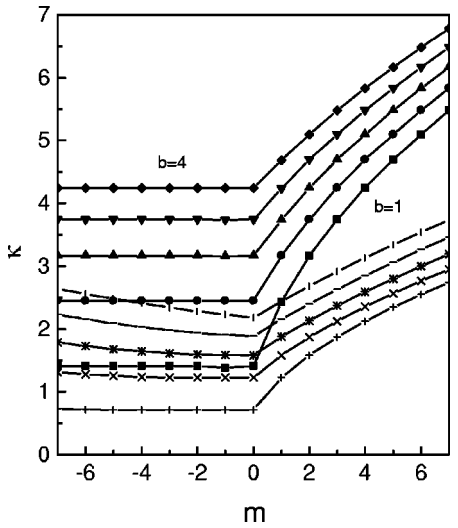


FIG. 4. Electron momentum as a function of the angular momentum $m$ for $b=1$ and $b=4$.

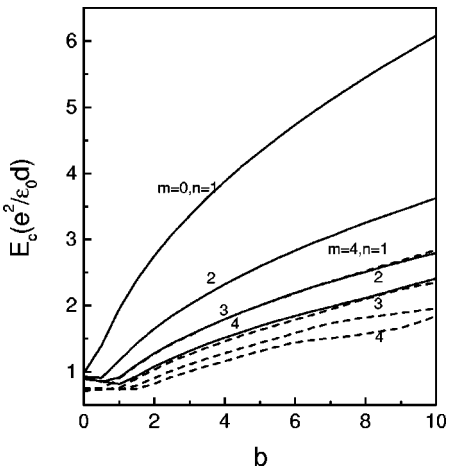


FIG. 5. Coulomb energies of two electrons as functions of the magnetic field $b$ for $m=0$ and $m=4$ states.

### C. Resonant tunneling properties

Figure 7 shows the transmission probabilities $T$ as functions of $\kappa$ for the circular dot structure with $\theta=\pi$, $0.5\pi$, and $0.75\pi$, respectively. Because $T$ varies by several orders of magnitude, we take $\log_{10}(T)$ as the ordinate. From Fig. 7, we see that $T$ shows a series of sharp peaks, which are similar to resonant tunneling peaks in usual quantum well structures

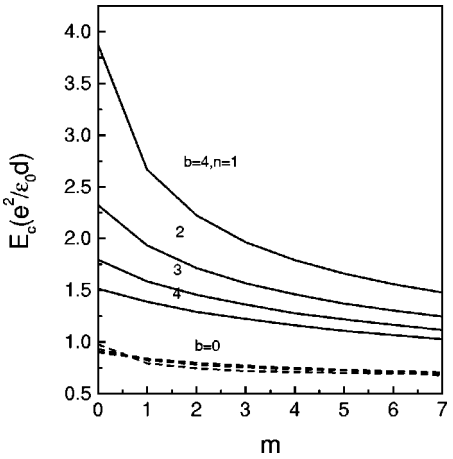


FIG. 6. Coulomb energies of two electrons as functions of the angular momentum $m$ for $b=0$ and $b=4$.

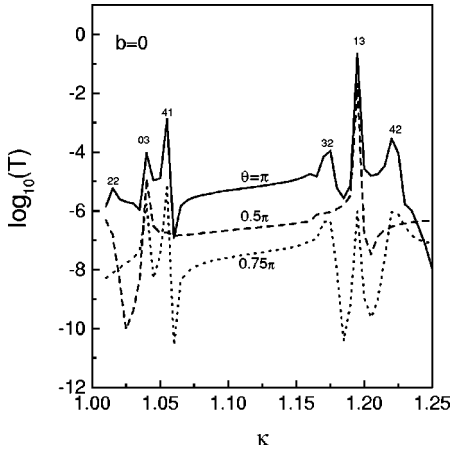


FIG. 7. Transmission probabilities as functions of the electron momentum $\kappa$ for the circular dot structure with $\theta=\pi$, $0.5\pi$, and $0.75\pi$ in $b=0$. The curves of $\theta=0.5\pi$ and $0.75\pi$ are shifted downwards in order for clarity.

with double potential barriers. It can be proved that the energy of the peaks corresponds to the energy of the bound states in the circular quantum dot. Comparing with Fig. 2, we can identify the peaks in Fig. 7 with the bound states in the circular dot, where the first number denotes the angular quantum number $m$ and the second number denotes the order of bound states.

Because the bound state in the circular dot has angular relation $e^{im\theta}$, we can use the $T$ values from the structures with different angles $\theta$ between the inject and exit channels to check the identification. For the case of $\theta=\pi/2$, $T$ has the angular relation $|\cos(m\pi/2)|^2$ which equals zero for $m=1,3,5,\ldots$, i.e., the resonance will not occur for these states. From Fig. 7, we see that all peaks with $m=1,3,5$ are restrained. Similarly for the case of $\theta=3\pi/4$, the resonance will not occur for states of $m=2,6,10,\ldots$. From Fig. 7, we also see that all peaks with $m=2,6$ are restrained.

Figure 8 shows $T$ as functions of $\kappa$ in the magnetic-field strength $b=0$, 1, and 4 for the circular dot with $\theta=\pi$. From

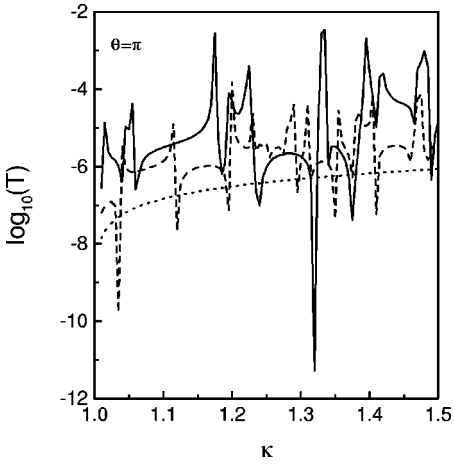


FIG. 8. Transmission probabilities as functions of the electron momentum $\kappa$ for the circular dot structure with $\theta=\pi$ in $b=0$ (solid line), $b=1$ (dashed line), and $b=4$ (dotted line).

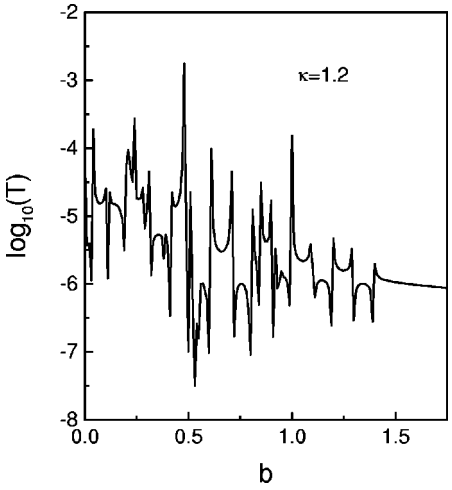


FIG. 9. Transmission probabilities as functions of the magnetic field $b$ for the circular dot structure with $\theta=\pi$ and electron momentum $\kappa=1.2$.

Fig. 8, we see that with the variation of the magnetic-field strength the position of the resonant peaks will change. At $b=4$, there is no resonant peak. There is also correspondence between the energies of the resonant peaks and bound states in quantum dot. From Fig. 4, we see that at $b=4$, the energies $(\kappa)$ of bound states increase so that only ground states of $-m$ states have the same energies $\kappa=1.413$, which lie in the range of $1<\kappa<2$. Figure 9 shows $T$ as functions of the magnetic field $b$ for $k=1.2$. From Fig. 9, we see that the height of the resonant peak decreases with $b$ increasing, and when $b\geqslant 1.5$ there is no resonant tunneling peak. The resonant peaks in the quantum dot do not have a definite period, unlike the $A$-$B$ ring. It is because that in the $A$-$B$ ring the oscillation of $T$ is caused by the magnetic flux through the ring, which makes the phase difference of electron waves traveling in up and down arms changing periodically. In the circular dot structures, the magnetic field changes the energy of bound states, resulting in the shift of the resonant peaks. Therefore the resonant tunneling in the circular dot structures can be used to study the bound states in the absence and presence of magnetic field.

## IV. SUMMARY

In this paper, we studied theoretically the ballistic transport in the semiconductor, planar, circular quantum dot structures. The transmission probabilities show apparent resonant tunneling peaks, which correspond to energies of bound states in the dot. By use of structures with different angles between the inject and exit channels, the resonant peaks can be identified very effectively. The perpendicular magnetic field has obvious effect on the energies of bound states in the quantum dot, and thus the resonant peaks. The treatment of the boundary conditions simplifies the problem to the solution of a set of linear algebraic equations. The theoretical results in this paper can be used to design planar resonant tunneling devices, whose resonant peaks are adjustable by the angle between the inject and exit channels and the applied magnetic field. The resonant tunneling in the circular

dot structures can also be used to study the bound states in the absence and presence of magnetic field. For example, we take the width of the channel, $d=20$ nm; the outside radius $r_2=60$ nm; the effective mass $m^*=0.067m_0$. Hence the energy unit $E_0=14$ meV, $b=0.4$ corresponds to the magnetic-field strength $B=3.25$ T. All these physical quantities are accessible experimentally with present nanometer-scale lithography technique and other techniques.

For the quantum dot of irregular shape, we can divide the region into many small segments. Each segment can be seen as a rectangular region with small width, and the total transfer matrix is evaluated by multiplication of the transfer matrices of all segments.[9] The effect of the soft wall is considered in Ref. 11, where the resonant peaks are shifted related to those in the hard wall case, but the whole structure has not changed. Therefore we expect that in our case for the soft wall potential, the confined energy will decrease somewhat and the resonant peaks are moved to the low momentum value.

## ACKNOWLEDGMENT

This work was supported by the Chinese National Science Foundation.

[1] J.M. Garcia, G. Medeiros-Ribeiro, K. Schmidt, T. Ngo, J.L. Feng, A. Lorke, and J. Kotthaus, Appl. Phys. Lett. **71**, 2014 (1997).
[2] R.J. Warburton, C. Schaflein, D. Haft, F. Bickel, A. Lorke, K. Karrai, J.M. Garcia, W. Schoenfeld, and P.M. Petroff, Nature (London) **405**, 926 (2000).
[3] A. Lorke, R.J. Luyken, A.O. Govorov, J.P. Kotthaus, J.M. Garcia, and P.M. Petroff, Phys. Rev. Lett. **84**, 2223 (2000).
[4] J.M. Llorens, C. Trallero-Giner, A. Garcia-Cristobal, and A. Cantarero, Phys. Rev. B **64**, 035309 (2001).
[5] J.B. Xia and S.S. Li, Phys. Rev. B **66**, 035311 (2002).
[6] B.J. van Wees, H. van Houten, C.W.J. Beenakker, J.G. Williamson, L.P. Kouwenhoven, D. Van der Marel, and C.T. Foxon, Phys. Rev. Lett. **60**, 848 (1988).
[7] D.A. Wharam, M. Pepper, H. Ahmed, J.E.F. Frost, D.G. Hasko, D.C. Peacock, D.A. Ritchie, and G.A.C. Jones, J. Phys.: Conden. Matter **21**, L209 (1988).
[8] F.A. Buot, Phys. Rep. **234**, 73 (1993).
[9] W.D. Sheng and J.B. Xia, J. Phys.: Condens. Matter **8**, 3635 (1996).
[10] Ch. Sikorski and U. Merkt, Phys. Rev. Lett. **62**, 2164 (1989).
[11] J.B. Xia and W.D. Sheng, J. Appl. Phys. **79**, 7780 (1996).